PHYSICAL REVIEW C VOLUME 8, NUMBER 2 AUGUST 1973

In-Beam Electron Conversion from Yrast Levels of ^{72,74,76,78}Se, ^{78,80,82,84}Kr, ^{114,116,118,120,122,124,126}Te, and ^{130,132,134,136,138}Ce Excited by (α, xn)†*

Walter G. Wyckoff‡ and James E. Draper
Crocker Nuclear Laboratory, University of California, Davis, California 95616
(Received 6 December 1972)

A new in-beam electron spectrometer was used to measure electron conversion intensities of cascade transitions between yrast levels of the nuclei listed above. A few $2+' \rightarrow 2+$ transitions were also measured. Altogether, 103 electron lines were measured during and between cyclotron bursts of 25–62-MeV α particles. The conversion coefficients, based on γ intensities from previous work at this laboratory, are compatible with the assignments of all but one of three transitions previously studied in this laboratory. The exception is the 1015-keV transition in ^{78}Kr, earlier obscured by a 1013-keV transition due to Al. These yrast level energies are correlated with a semi-empirical model. The complementary nature of measurements of in-beam angular distributions of γ rays and measurements of electron conversion coefficients is discussed.

NUCLEAR REACTIONS ^{70}Ge$(\alpha,2n)$, E=27.5 MeV, ^{72}Ge$(\alpha,2n)$, E=27.5 MeV, ^{74}Ge$(\alpha,2n)$, E=27.5 MeV, ^{76}Ge$(\alpha,2n)$, E=27.5 MeV, ^{76}Se$(\alpha,2n)$, E=27.5 MeV, ^{78}Se$(\alpha,2n)$, E=25 MeV, ^{80}Se$(\alpha,2n)$, E=25 MeV, ^{82}Se$(\alpha,2n)$, E=25 MeV, ^{112}Sn$(\alpha,2n)$, E=33 MeV, ^{114}Sn$(\alpha,2n)$, E=27.5 MeV, ^{116}Sn$(\alpha,2n)$, E=33 MeV, ^{118}Sn$(\alpha,2n)$, E=27.5 MeV, ^{120}Sn$(\alpha,2n)$, E=27.5 MeV, ^{122}Sn$(\alpha,2n)$, E=27.5 MeV, ^{124}Sn$(\alpha,2n)$, E=25 MeV, ^{130}Ba$(\alpha,4n)$, E=62 MeV, ^{130}Ba$(\alpha,2n)$, E=33 MeV, ^{134}Ba$(\alpha,4n)$, E=62 MeV, ^{136}Ba$(\alpha,4n)$, E=62 MeV, ^{136}Ba$(\alpha,2n)$, E=27.5 MeV; measured in-beam ce intensities of transitions between yrast levels; from earlier γ intensities deduced ce coefficients to test level assignments; compared usefulness of angular distributions and ce coefficients; compared yrast level energies with EXP model.

Previous in-beam γ spectroscopy work by our group,[1-4] including γ angular distributions, has gone far to establish the quasirotational level structure in the even-even nuclei ^{72,74,76,78}Se, ^{78,80,82,84}Kr, ^{114,116,118,120,122,124,126}Te, and $^{130\ 132\ 134\ 136\ 138}$Ce. The intent of the present work is to test these level assignments with in-beam measurements of electron internal conversion coefficients (denoted ICC) during (α, xn) reactions.

Previously the assignments of levels used the angular distributions[1-4] of the γ rays. These are caused by the alignment of the nucleus since only the M = 0 substate (z axis along the cyclotron beam) is produced initially by the capture of the α particle. The interpretation of these angular distributions is not unambiguous and there are several combinations of spins which produce similar angular distributions. In the measurement of ICC's different ambiguities appear—e.g. the close similarity of the conversion coefficients of M1 and E2. In Sec. V these two methods are compared and shown to be complementary.

I. EXPERIMENTAL METHOD

The α-particle beams used in this experiment were produced by the 76-in sector-focusing isochronous cyclotron of this laboratory. The α energy from this machine is variable from 22 to 86 MeV, and beam currents up to several hundred nanoamps were focused onto the 1-cm target.

Conversion electrons were detected by a 3-mm-deep Si(Li) detector behind a short solenoidal lens with helical positron-inhibiting vanes. The system has a resolution capability of 2.5 keV full width at half maximum FWHM for 500–700-keV electrons and a useful electron energy range of 50–1800 keV. The system including solenoid has an efficiency ~50 times larger than when the solenoid and vanes are removed. The solenoid and baffle reject heavy particles, positrons, δ rays, x rays, and most γ rays. A detailed description of this spectrometer will be given elsewhere.[5] The spectrometer was used at 90° from the α beam.

Targets were made from isotopically enriched powders of germanium oxide, selenium metal, tin oxide, and barium carbonate or nitrate. These powders were deposited from a slurry onto 0.0006-cm aluminized Mylar. The targets ranged in thickness from 0.5 to 6 mg/cm^2, resulting in energy resolutions of 2.5 to 8 keV FWHM in the 500- to 700-keV electron range. Target making techniques are described in Ref. 5.

Data were accumulated in two modes. The first was a two-parameter time sorting. Spectra of counts vs pulse height were collected in eight bands of 512 channels according to time after the beam pulse ($\lesssim 3$ nsec wide at ~8-MHz rate) had passed through the target. This helped to identify half-lives and to optimize the ratio of signal to noise for longer-lived transitions. The second mode was a single-parameter spectrum, counts vs pulse height, where 4096 channels were used with very thin targets to maximize energy resolution. Details of the electronics are given in Refs. 1–4.

The electron spectrometer was calibrated using a thin ^{152}Eu source, which has well-studied conversion electron lines from 75 to 1360 keV. This source provided calibration of both energy and relative efficiency using the electron data of Malmsten, Nilsson, and Anderson.[6]

The position of the peak was taken to be the channel with the greatest number of counts for the high-resolution spectra. This channel was nearly in the center of the almost symmetric peak. This led to an energy determination which was frequently low by about 1.5 keV, the expected average energy loss in the target. For the thicker targets the fairly sharp high-energy edge was used as the peak position. This led to energies which were low by 1 to 2 keV for the same reason. The energies of the K and L electrons, after making these corrections and adding the binding energy of the electron, agreed well with the previously measured γ energies.[1-4] For the K electrons there were 66 lines within ±0.5 keV, 16 additional lines within ±1.5 keV, and the remaining 3 lines were within ±2.5 keV of agreement.

The beam energies were chosen to match the beam energies used in the γ-ray research.[1-4] The γ-ray targets were 5 to 10 times thicker than the electron targets, leading to beam energy losses of 2 to 6 MeV in passing through them. Consequently, the beam energies used in the electron work were decreased so that the beam energies at the centers of the targets were the same for the electron and γ data. Compromises were made to reduce the number of different beam energies needed, but all were kept to within ~2 MeV of the corrected γ-run beam energies. The γ intensities do not change significantly ($\lesssim 4\%$) over this range. The results of Refs. 1–4 were used for the relative γ-ray intensities.

Figures 1–3 are examples of the electron spectra taken for this work. Figure 1 illustrates the line shape for a strong electron line—viz., a new $0 \to 0$ monopole electron from a 937-keV state in

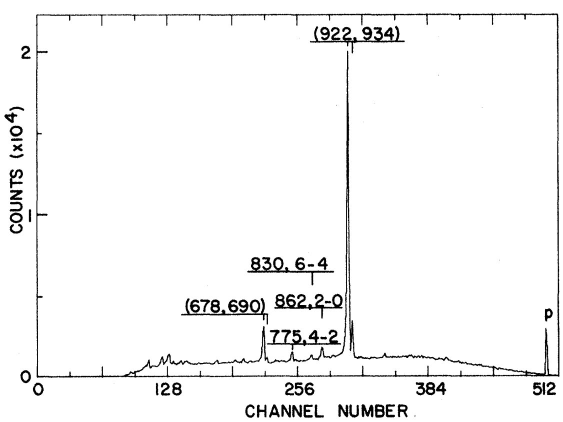

FIG. 1. Conversion electron spectrum from $^{70}Ge(\alpha, 2n)$-^{72}Se at 27.5 MeV. The labels not in parentheses are transition energies and assignments. The peaks labeled (922, 934) and (678, 690) are $E0$ transitions between 0+ states. The peak labeled P is from a pulser. This spectrum is the sum of eight time bands of 512 channels, each, like Fig. 2.

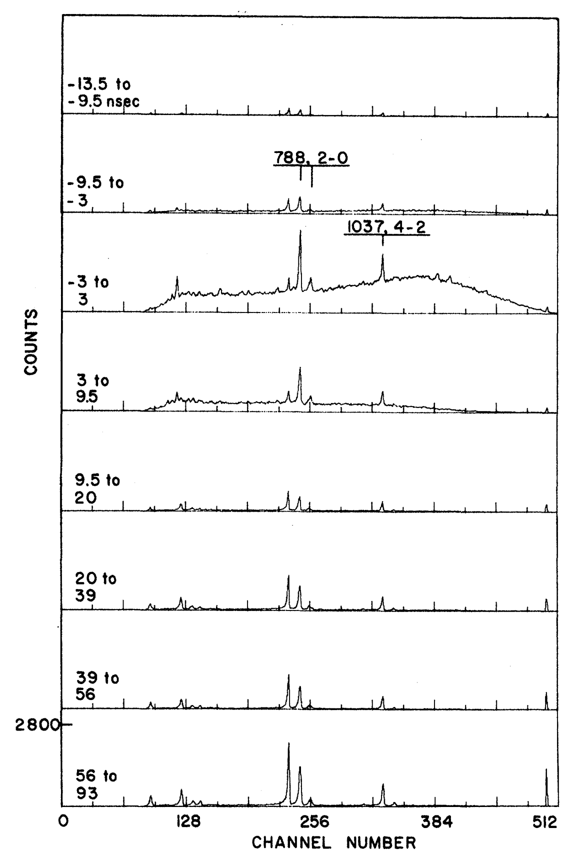

FIG. 2. Timing spectra of electrons from $^{136}Ba(\alpha, 2n)$-^{138}Ce. The third spectrum from the top was taken during the 6-nsec encompassing the beam burst. The timing of each band is listed on its left side. The various half-lives are clearly evident as is the disappearance of the continuum after the beam burst.

^{72}Se, discussed below. Figure 2 illustrates data sorted into time bands ranging from 6-nsec width near the α beam burst to 37 nsec for a late band. The large continuum (real) during the beam burst and the differences in half-lives of various lines are apparent. Figure 3 illustrates part of a 4096-channel spectrum with 2.8-keV resolution. In the complete set of data there are 20 nuclei for which a two-parameter 512 ×8-channel timing spectrum was obtained. In addition, high-resolution 4096-channel singles spectra were obtained for eight nuclei.

The electron data were normalized to the 2→0 transition in each nucleus, i.e., it was assumed that this transition was correctly identified as an E2 transition. Then using the theoretical ICC of $\alpha_K(2\to0)$ from Hager and Seltzer[7] the experimental K electron conversion coefficient was obtained as

$$\alpha=(I_e/I_{e\,2\to0})\,(I_\gamma/I_{\gamma\,2\to0})^{-1}\,\alpha_K(2\to0)f_\theta\ , \qquad (1)$$

where I denotes the relative intensity of γ rays or electrons corrected for the energy dependence of the detector efficiency. The factor f_θ corrects for the effect of the angular distribution of the in-beam electrons with respect to the α-beam direction.

II. CORRECTION FOR ELECTRON ANISOTROPY

Since the α beam produces compound nuclei in the $M=0$ substate of angular momentum for even-even targets, the nucleus is strongly aligned when it emits the electron. This results in substantial anisotropy of the electron angular distribution. Draper and Johnsen[8] have calculated this electron angular distribution, $W_e(\theta)$. Their work was based on that of Steffen.[9] The electron angular distributions of Ref. 8 were based on a Gaussian distribution of substates of a level J with the Gaussian width σ given as

$$\sigma=1.6+(J/10) \qquad (2)$$

in keeping with results of Ref. 10.

The correction f_θ in Eq. (1) is obtained by calculating the ratio of $\int_0^\pi[W_e(\theta)/W_e(\pi/2)]\sin\theta\,d\theta$ for the transition in question compared to that of the 2→0. The resulting correction factors are listed in Table I. The corrected experimental ICC's are plotted in Fig. 4.

III. K/L RATIOS

For lower-energy transitions and larger Z the K/L ratios (integrated electron intensity from K shell divided by the integrated electron intensity from the total L shell) are useful in determining multipolarity. However, for the transitions in this work the K/L ratios are much less sensitive to multipolarity than is the K conversion coefficient. For example, for $Z=34$ and $E_\gamma \gtrsim 500$ keV the K/L ratios[7] of all of $E1$ to $E4$ and $M1$ to $M4$ transitions are the same within ±8%. For $Z=52$ the K/L ratios of all of $M1$, $E1$, $M2$, $E2$, and $M3$ are independent of multipolarity within ±13%. In Fig. 4 is evident a much stronger dependence of α_K on multipolarity. As for distinguishing $M1$ and $E2$, those K/L ratios differ by no more than 8% for any transition in this work. This is not sufficient to be useful.

Since the K/L ratios are ~7 to 10 for these transitions the intensities of L transitions are much more uncertain than the intensities of the K transitions. This adds to the problem of the insensitivity of K/L ratios to multipole character.

In every case where the L transition was sufficiently resolved and sufficiently intense (i.e., for ~30 transitions) the experimental K/L ratio was determined. There was no case of a conflict with the assignments made from the K conversion coefficients. Consequently the K/L ratios are not

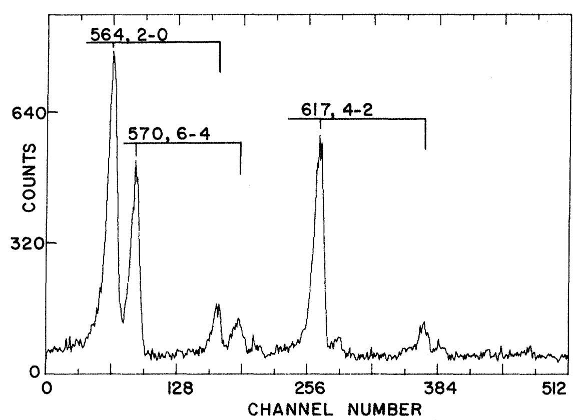

FIG. 3. Part of a higher-resolution (4096 channels) electron spectrum from ^{120}Sn(α, 2n)^{122}Te. With this thinner target the peak width is 2.8 keV. The spectrum covers all time during and between the beam bursts.

TABLE I. Correction factor f_θ, Eq. (1), for differences in angular distributions of electrons for various transitions. The f_θ is essentially the same for K and L electrons, L_{II} and L_{III} conversion being weak.

Transition	f_θ
2+ → 0+	1
4+ → 2+	1.08
6+ → 4+	1.14
8+ → 6+	1.16
10+ → 8+	1.17
2+ → 2+ ($E2$ or $M1$)	0.83

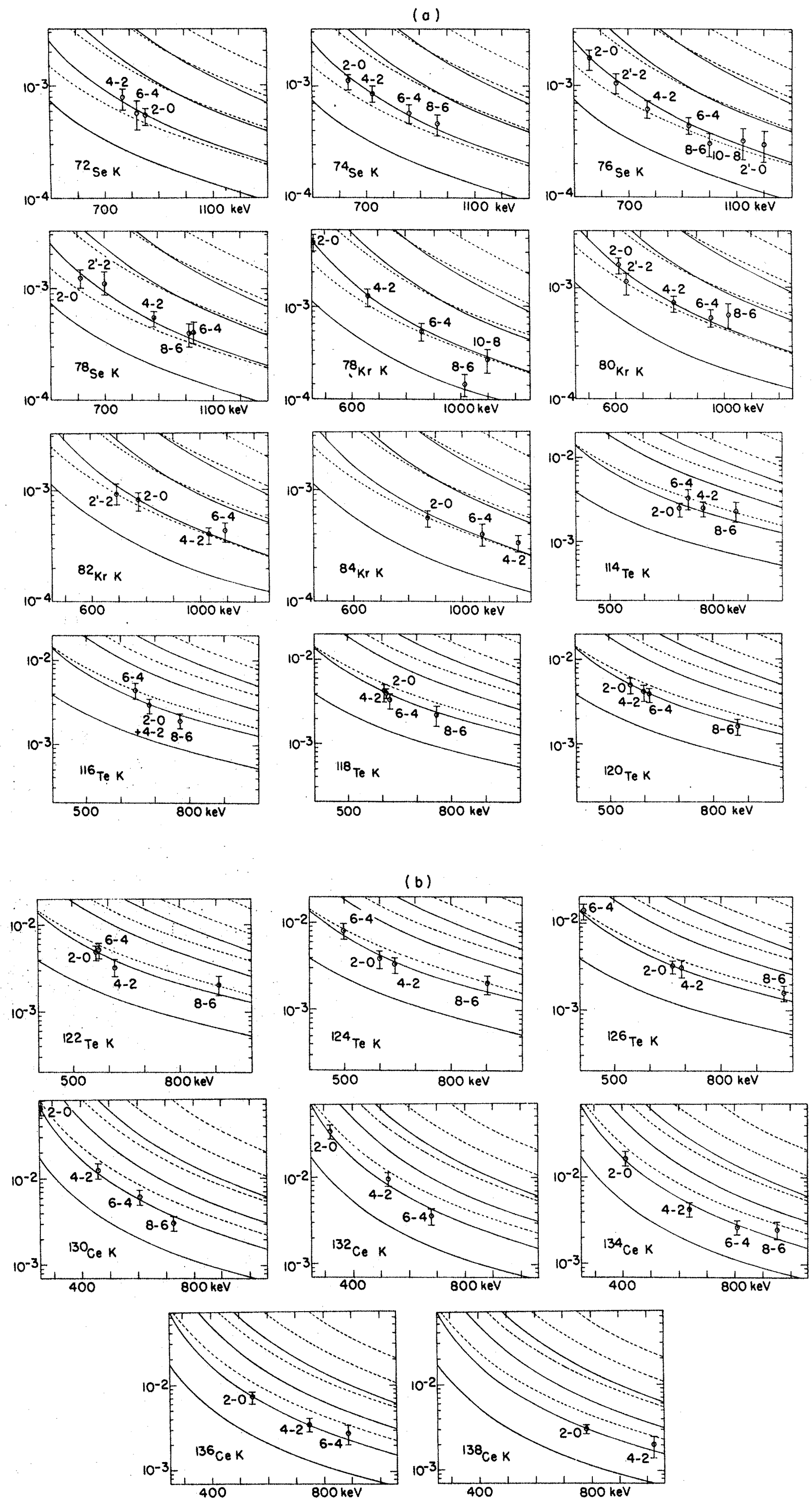

FIG. 4. (a), (b) Composite of K conversion results. The solid curves are theoretical values of the K conversion coefficient for, from bottom to top, $E1$, $E2$, $E3$, and $E4$. The dashed curves, from bottom to top, are $M1$, $M2$, $M3$, and $M4$.

TABLE II. Relative intensities of electrons at 90° from the beam. The correction f_θ, Table I, has not been applied here.

Transition energy (keV) [a]	K electron intensity [b]
^{72}Se	
691	340 (25)
775(4 → 2)	88 (15)
830(6 → 4)	38 (20)
862(2 → 0)	100 (15)
935	2340 (15)
^{74}Se	
635(2 → 0)	100 (15)
691	125 (15)
728(4 → 2)	48 (15)
868(6 → 4)	17.5 (15)
935	9.0 (20)
966(8 → 6)	7.9 (20)
^{76}Se	
560(2 → 0)	100 (15)
658(2′ → 2)	11.8 (15)
691	4.5 (15)
772(4 → 2)	22.5 (15)
932(6 → 4)	7.1 (15)
1008(8 → 6)	3.1 (20)
1131(10 → 8)	1.6 (20)
1216(2′ → 0)	2.2 (20)
^{78}Se	
613(2 → 0)	100 (15)
693(2′ → 2)	25 (20)
886(4 → 2)	29 (15)
935	36 (15)
1036(8 → 6)	5.9 (20)
1040(6 → 4)	11.7 (20)
^{78}Kr	
454(2 → 0)	100 (15)
664(4 → 2)	23.5 (15)
858(6 → 4)	8.3 (15)
1015(8 → 6)	2.10 (20)
1110(10 → 8)	1.32 (20)
^{80}Kr	
617(2 → 0)	100 (15)
640(2′ → 2)	14.3 (15)
820(4 → 2)	35 (15)
956(6 → 4)	12.6 (15)
1017(8 → 6)	6.0 (20)
^{82}Kr	
698(2′ → 2)	19 (15)
777(2 → 0)	100 (15)
1044(4 → 2)	27.5 (15)
1099(6 → 4)	12 (15)
^{84}Kr	
881(2 → 0)	100 (15)
1078(6 → 4)	15.5 (20)
1214(4 → 2)	23 (15)
^{114}Te	
280	530 (15)
322	380 (15)
708(2 → 0)	100 (15)
733(6 → 4)	63 (15)
775(4 → 2)	67 (15)
871(8 → 6)	23 (20)
^{116}Te	
643(6 → 4)	52 (15)
679 + 681, 2 → 0 + 4 → 2	100 (15)
771(8 → 6)	8.7 (15)
^{118}Te	
601(4 → 2)	100 (15)
606(2 → 0)	100 (15)
615(6 → 4)	41 (15)
754(8 → 6)	13 (15)
^{120}Te	
560(2 → 0)	100 (15)
601(4 → 2)	62 (15)
615(6 → 4)	35 (15)
877(8 → 6)	5.3 (15)
^{122}Te	
564(2 → 0)	100 (15)
570(6 → 4)	50 (15)
617(4 → 2)	54 (15)
915(8 → 6)	8.2 (15)
^{124}Te	
499(6 → 4)	98 (15)
603(2 → 0)	100 (15)
646(4 → 2)	65 (15)
917(8 → 6)	11.5 (15)
^{126}Te	
414(6 → 4)	190 (15)
665(2 → 0)	100 (15)
694(4 → 2)	89 (15)
989(8 → 6)	6.7 (15)
^{130}Ce	
253(2 → 0)	100 (15)
456(4 → 2)	14 (15)
614(6 → 4)	6.3 (15)
729(8 → 6)	2.0 (15)

TABLE II *(Continued)*

Transition energy (keV) [a]	*K* electron intensity [b]	Transition energy (keV) [a]	*K* electron intensity [b]
^{132}Ce		Additional strong lines, identified by *electron energies* (in parentheses).	
326(2→0)	100 (15)	^{118}Te	
534(4→2)	21 (15)	(301)	27.5 (15)
684(6→4)	4.9 (15)	^{130}Ce	
^{134}Ce		(252)	78 (15)
409(2→0)	100 (15)	(324)	27 (15)
640(4→2)	25 (15)	(508)	5.6 (18)
815(6→4)	9.2 (15)	(630)	3.5 (18)
947(8→6)	4.2 (15)	(711)	4.0 (18)
^{136}Ce		^{134}Ce	
552(2→0)	100 (15)	(347)	83 (15)
762(4→2)	43 (15)	^{136}Ce	
899(6→4)	6.3 (20)	(388)	120 (15)
^{138}Ce		(547)	225 (15)
788(2→0)	100 (15)	(656)	79 (15)
1037(4→2)	53 (15)	(681)	80 (15)

[a] $J_i \to J_f$ assignments from Refs. 1–4 in parentheses.

[b] Uncertainty in percent given in parentheses.

listed here since they would not contribute new information.

IV. RESULTS

Table II lists the transitions studied, including some of the stronger unassigned lines. All relative intensities from the two-parameter data were calculated from the summed spectra. Where both two-parameter and singles spectra were taken, the relative intensities listed in Table II are the averages.

In order to facilitate comparison of the experimental ICC's with the theoretical values, Fig. 4 shows the assembled results. The theoretical conversion coefficients are from Hager and Seltzer.[7] The error bars in Fig. 4 include, in quadrature, the uncertainty in the γ relative intensity from Refs. 1–4, the statistical uncertainty in the electron peak area, and the uncertainty in relative efficiency for the electron system at the 2→0 energy and the energy in question.

Included in Fig. 4 is the conversion coefficient of the 2→0 transition for each nucleus. This is the reference point for calculating the other coefficients as in Eq. (1). The error bar for the 2→0 transition has a special significance, since any deviation in the strength of the 2→0 transition (γ or electron) changes all other conversion coefficients for that nucleus by the *same* factor. The error bar on the 2→0 conversion coefficient indicates the range over which all ICC's for that nucleus can be translated as a group. It would be misleading to incorporate this uncertainty of the 2→0 transition into the lengths of the other error bars since those individual error bars would no longer be statistically uncorrelated. The present method conveys more information.

^{72}Se

The strong 922-keV electron in Fig. 1 is an $E0$ transition from a new[11] 0+ state in ^{72}Se. This tentative identification, as well as that of the 678-keV electron as resulting from a 0→0 transition in ^{72}Ge resulting from $(\alpha, 2p)$, has been confirmed by subsequent accurate measurements[12] of the K-L energy separations of both lines (for isotopic identification) and the half-life of the 678-keV line using an α-beam sweeper.

^{74}Se

The 635-keV 2→0 transition will include some weak admixture of a 2′→2 transition in ^{74}Se at the same energy[13] (within $\lesssim$1 keV). However the latter, in addition to being weak, also has nearly the same α_K as the former so the effect will be negligible.

^{76}Se

In addition to the $10\rightarrow 8\rightarrow 6\rightarrow 4\rightarrow 2\rightarrow 0$ cascade being compatible with $E2$ the $2'\rightarrow 2$ and $2'\rightarrow 0$ are compatible with $E2$ in Fig. 4. In Ref. 14 a possible 0+ state at 1123 keV is reported. This energy is so far above that of the 2+ state that the branching ratio $(0\rightarrow 2)/(0\rightarrow 0)$ would be unfavorable for observing the $0\rightarrow 0$ transition. This is to be contrasted with Fig. 1 where the $0\rightarrow 0$ transition is prominent.

^{78}Kr

The ICC's for the $10\rightarrow 8$, $6\rightarrow 4$, and $4\rightarrow 2$ transitions in Fig. 4 support the $E2$ assignments of Ref. 2. However, the previously assigned $8\rightarrow 6$ appears here to have an ICC appropriate to $E1$. As noted in Ref. 2 the angular distribution of this 1015-keV γ ray was obscured by the 1013-keV line from Al in the beam pipe and required a different type of analysis. The character of that angular distribution rests on the 90° point in Fig. 5 of Ref. 2. The excitation function of the 1015-keV transition in Ref. 2 also was the least satisfactory among the 15 transitions studied there, and there was a dead-time problem described therein for that transition. Of course, the conversion electron for the 1013-keV transition in Al would not be observed here because α_K is small, and the Al was some distance downstream from the electron spectrometer. The discrepancy occurs either because the angular distribution of Ref. 2 is incorrect or because the relative γ intensity used in α_K is $\gtrsim 70\%$ too large.

Several experiments[15] have suggested a 0+ state near the 4+ state. This is far enough above the 2+ state that negligible $0\rightarrow 0$ intensity would be expected.

^{80}Kr

The ICC's in Fig. 4 are consistent with $E2$, including that for the 1017 keV, $8\rightarrow 6$ transition at which energy the aluminum γ line caused interference in Ref. 2 as discussed above.

^{84}Kr

A possible 0+ state at 2171 keV[16] is too far above the 2+ state to produce significant $0\rightarrow 0$ intensity from electron conversion.

^{116}Te

It was not possible to separate reliably the very close doublet, $2\rightarrow 0$ and $4\rightarrow 2$, separated by 2 keV. Therefore the other coefficients were found by normalization to the sum of these peaks. The K and the L ICC's agree well with an $E2$ multipolarity for $6\rightarrow 4$ and $8\rightarrow 6$.

There is no evidence for the 509-keV first 2+ state assigned by Spejewski, Hopke, and Loeser.[17]

^{120}Te

The possible 1103-keV 0+ state observed by Spejewski, Hopke, and Loeser,[17] would be too far above the 2+ state to give appreciable $0\rightarrow 0$ electron intensity.

^{122}Te

Kerek[18] assigns a tentative $10+\rightarrow 8+$ γ transition at 622 keV with an intensity 0.12 times that of the 617-keV transition at an α energy of 23 MeV. This α energy is similar to our 27.5 MeV. In Fig. 3 there is a suggestion of this peak in the electron spectrum with roughly the correct intensity for $E2$. A longer electron run would yield more quantitative results.

^{124}Te

A $10+\rightarrow 8+$ transition at 490 keV with an intensity 0.3 times that of the 498-keV transition (23-MeV α particles) is reported by Kerek.[18] Our electron spectrum shows a weak peak at the appropriate energy with approximately the intensity for an $E2$ transition when the γ intensity of Ref. 18 is used.

Recent experiments with radioactive decay[19,20] to ^{124}Te have reported 0+ levels at 1156, 1658, and 2020 keV. In Ref. 19 $E0$ electrons of 1156, 1658, (1658-1156), and (2020-1156) keV are reported. These were too weakly excited to be observable in the relatively short run made here. Another 0+ state at 1290 keV is reported[21] from (d, d'), but it was not observed in this short run.

^{126}Te

The $8+\rightarrow 6+$ transition at 989 keV, reported earlier[3] is confirmed here to have an ICC compatible with $E2$. The 13-nsec 209-keV transition feeding this 8+ state[3] has recently been assigned[18] as $10+\rightarrow 8+$ on the basis of angular distribution following $(\alpha, 2n)$. Unfortunately, the energy range over which the solenoid was swept did not include this 209-keV transition.

In Ref. 19 0+ levels at 1396, 1685, and 2061 keV are reported but the $E0$ transitions were not observed in this short run.

^{132}Ce

Considering the γ relative intensities of Ref. 4, the theoretical $E2$ conversion coefficients, and the electron relative efficiencies, the uncertain $10\rightarrow 8$

K electron should have a counting rate 0.15 times that of the $6\rightarrow4$ electron. This $10\rightarrow8$ electron was not definitely observed in the present work, but it could have just been obscured by statistics in the spectrum. The $8\rightarrow6$ K electron was obscured by the L line of the $M4$ transition in ^{139}Ce due to the unusually large impurities of ^{137}Ba and ^{138}Ba in this target. The ICC's of the $6\rightarrow4$ and $4\rightarrow2$ transitions are consistent with Ref. 4.

^{134}Ce

The ICC's are compatible with an $E2$ assignment for the transitions of Ref. 4 including the uncertain $8\rightarrow6$ transition.

^{138}Ce

This nucleus is well studied, including the conversion electrons. The ICC's here check the method. The most recent decay scheme[22] of ^{138}Ce shows a 0+ state at 1477 keV with 3% of its disintegrations going by $E0$ to ground. This energy was on the upper tail of the solenoid pass band.

V. COMPLEMENTARITY OF ICC'S AND ANGULAR DISTRIBUTIONS

A primary basis of the earlier assignments[1–4] of levels is that the angular distributions of the γ rays were compatible with stretched $E2$ cascades down the yrast states (i.e., lowest energy for a given spin-parity $J\pi$) of $J\pi = 0+,\ 2+,\ 4+,\ 6+, \ldots$. However, there is a problem. There are other combinations of level spins and transition multipolarities which give γ-ray angular distributions sufficiently similar to those of stretched $E2$ that they may not be ruled out with data on angular distributions alone.

The results of the present experiments, Fig. 4, are that all but one of the transitions under consideration have ICC's appropriate to $M1$ and/or $E2$ with slight preference for $E2$ where they are somewhat distinguishable.

Let us then briefly consider the question of the limitations imposed on the level spins and multipole character of the radiation when both ICC's and angular distributions of the γ rays have been measured. More specifically, how do experiments giving angular distributions compatible with $E2$ and experiments giving ICC's compatible with $M1$ and/or $E2$ complement each other? The following angular distributions have been calculated[23] here for the transition $J_i\,(L1, L2)J_f$ with an assumed Gaussian distribution[24] of population of M states for the initial state J_i: $J(3,3)J-3$, $J(2,2)J-2$, $J(2,3)J-2$, $J(3,3)J-2$, $J(1,1)J-1$, $J(1,2)J-1$, $J(2,2)J-1$, $J(1,1)J$, $J(1,2)J$, and $J(2,2)J$ for $J=1,2,3,\cdots10$.

These were calculated with an $L2/L1$ mixing ratio of $\delta = 0.01,\ 0.1,\ 1,\ 10,\ 100$. The resulting compilation is too massive to tabulate in a publication. Of those cases above, which of course are not exhaustive, the following angular distributions could be confused with stretched $E2$ [i.e., $J(2,2)J-2$] because of experimental and statistical uncertainties and the lack of direct knowledge of the width of the Gaussian substate population. Those which could be confused with stretched $E2$ are: (a) $J(3,3)J-3$, i.e., stretched octupole. (b) $J(2,3)J-2$ in a wide range of mixtures ($\delta = 0.01$, 0.1, 10, and 100) of quadrupole and octupole including pure octupole. Also included is the case of an equal mixture of quadrupole and octupole radiation ($\delta = 1$) when the nucleus is not too strongly aligned. (c) $J(1,2)J-1$ with an equal mixture of dipole and quadrupole ($\delta = 1$). (d) $J(1,1)J$. (e) $J(1,2)J$ with mixtures from pure quadrupole to an equal mixture of dipole and quadrupole ($\delta = 1, 10, 100$).

On the other hand, the present experimental results show that all of the transitions except the 1015-keV transition in ^{78}Kr are primarily $E2$ and/or $M1$ with $E2$ more favored for the heavier nuclei. These results eliminate the categories of (a), stretched octupole and (d) with $E1$. They also eliminate (b) if $\delta \lesssim 0.1$. They also eliminate any cases not calculated in Ref. 23 (e.g., those for $J_f > J_i$) which have angular distributions similar to stretched $E2$ and/or $M1$.

From the other point of view, starting from the present experimental results on ICC's (i.e., $M1$ and/or $E2$) our experimental angular distributions would eliminate from the cases calculated in Ref. 23 the following: (1) $J\rightarrow J-1$ with predominantly $M1$; (2) $J(M1, E2)J-1$ with all mixing ratios; (3) $J\rightarrow J-1$ with pure $E2$; and (4) $J(M1, E2)$-J with predominantly $E2$.

In summary, the in-beam experiments on γ-ray angular distributions and those on conversion electrons are both necessary and complementary, each eliminating a large number of possible spin combinations.

VI. PARAMETRIZATION OF LEVEL ENERGIES

There have been several semiempirical models for the energies of rotational and quasirotational levels of nuclei. The only two with a minimum of parameters which give fairly accurate results for a wide variety of nuclei are called VMI (variable moment of inertia[25]) and EXP (expotential moment of inertia[26]). It is of interest to parametrize the energies of the quasirotational levels of the present experiment to quantify the smoothly varying nature of the patterns of level energies and further reveal the quasirotational nature of their level energies.

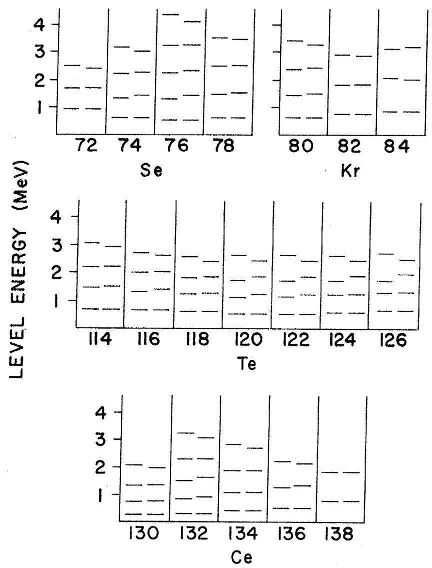

FIG. 5. Experimental yrast level energies, on the left, and from the EXP model, Eq. (3), on the right. In each case the sequence is 0+, 2+, 4+, 6+, ... starting from the ground state.

TABLE III. Values of the stiffness parameter S, the reference moment of inertia $\mathscr{I}_0$, and the equilibrium ρ for $J=2$, $\rho(2)$, in the EXP model, Eq. (3), for best fit to nuclei in present work.

Nucleus	S	$2\mathscr{I}_0/\hbar^2$ (MeV^{-1})	$\rho(2)$
^{72}Se	0.73	3.3	3.4
^{74}Se	2.7	6.7	1.8
^{76}Se	5.7	8.8	1.4
^{78}Se	5.2	7.9	1.5
^{80}Kr	4.0	7.5	1.6
^{82}Kr	3.2	5.7	1.7
^{84}Kr	2.8	4.9	1.8
^{114}Te	1.6	5.2	2.3
^{116}Te	1.2	5.0	2.6
^{118}Te	1.3	5.8	2.5
^{120}Te	1.9	7.0	2.1
^{122}Te	1.9	6.9	2.1
^{124}Te	1.4	6.0	2.4
^{126}Te	1.1	4.9	2.8
^{130}Ce	18	22	1.2
^{132}Ce	12	17	1.2
^{134}Ce	9.0	13	1.3
^{136}Ce	4.1	8.4	1.6
^{138}Ce	2.7	5.4	1.8

The EXP model equation[26] is

$$\epsilon(J)=\{S(\ln\rho)^2+J(J+1)/\rho\}_{\min} \qquad (3)$$

and the VMI model equation[25] is

$$\epsilon(J)=\{C\mathscr{I}_0^{\,3}(\rho-1)^2+J(J+1)/\rho\}_{\min}\,, \qquad (4)$$

where $\rho=\mathscr{I}/\mathscr{I}_0$, $\mathscr{I}$ is the moment of inertia, and the notation $\{\}_{\min}$ means the minimum as ρ is varied and J, the level spin, is fixed. The level energy $\epsilon(J)$ is in appropriate units [see Eq. (5)], since only energy ratios are of interest here. Each of Eqs. (3) and (4) is a one-parameter model for energy ratios relative to the energy of the 2+ state, the parameter being S or $C\mathscr{I}_0^{\,3}$, since ρ is determined by the minimization. Equation (4) is a special case of Eq. (3) for ρ near unity.

The experimental data for yrast levels of nuclei throughout the Periodic Table cover the span $J(J+1)/6 \gtrsim E(J)/E(2) \gtrsim 1$. The former are rigid rotors. The latter are magic or doubly magic. This full region is covered smoothly by EXP, the stiffness parameter S ranging montonically[26] from $+\infty$ to 0. The microscopic meaning of S is discussed in Ref. 26.

The original VMI model[25] covered the range $\frac{10}{3} \gtrsim E(4)/E(2) \gtrsim 2.23$ as $C\mathscr{I}_0^{\,3}$ ranges from $+\infty$ to 0. This would exclude all Te nuclei here, as well as ^{72}Se and ^{74}Se. Later it was reported[27] that as $C\mathscr{I}_0^{\,3}$ ranges from 0 to $-\infty$ the region $2.23 \gtrsim E(4)/E(2) \gtrsim 1.82$ is covered by Eq. (4). The physical significance of $C\mathscr{I}_0^{\,3}$ as it ranges over $+\infty$ to $-\infty$ in VMI is not transparent. There is no solution of Eq. (4), VMI, for the range $1.82 \gtrsim E(4)/E(2) \gtrsim 1$ appropriate to magic or near-magic nuclei.

Since the experimental level energies in Fig. 4 exhibit a smoothly varying pattern, we have chosen to parametrize this with the smoothly varying parameters and patterns of the EXP model of Eq. (3). The expression in terms of $\epsilon(J)$ produces the simplest form. However the actual level energy $E(J)$ is given[26] by

$$E(J)=\epsilon(J)\,\hbar^2/2\mathscr{I}_0\,. \qquad (5)$$

Thus, for each nucleus the experimental energy of the first 2+ state was set equal to $\epsilon(2)\hbar^2/2\mathscr{I}_0$, and S was varied to obtain the minimum value of

$$\sum_J [E_{\mathrm{expt}}(J)-E(J)]^2/E^2(J) \qquad (6)$$

using Eqs. (3) and (5) for $E(J)$. This determines the proper S and $\mathscr{I}_0$ as well as the equilibrium ρ for each spin J. The results are shown in Fig. 5. The parameters are given in Table III, including $\rho(2)$, the value of $\mathscr{I}/\mathscr{I}_0$ for $J=2$.

One sees that large values of S accompany nuclei which have ratios of level energies most nearly like $J(J+1)$ as in the rigid rotor. The largest S is for ^{130}Ce which appears in Fig. 5 to have energy ratios most like a rigid rotor. The ratio $\mathscr{I}(2)/\mathscr{I}_0 = \rho(2)$ exceeds 3 for the softest nucleus ^{72}Se but is only 1.2 for the stiffest nucleus ^{130}Ce. As seen in Eq. (5) the parameter $\mathcal{J}_0$ is closely related to the energy $E(2)$ in an inverse relation. The $\mathcal{J}_0$ depends only weakly on S.

ACKNOWLEDGMENTS

It is a pleasure to thank Dr. Nick King for his very useful assistance during parts of the data acquisition. The cyclotron crew were also very helpful.

---

†Work supported in part by the National Science Foundation.

*In part from the Ph.D. dissertation of W. G. W.

‡Present address: Medical Radiation Physics, University of Washington, Seattle, Washington 98105.

[1]R. M. Lieder and J. E. Draper, Phys. Rev. C 2, 531 (1970).

[2]D. G. McCauley and J. E Draper, Phys. Rev. C 4, 475 (1971).

[3]R. A. Warner and J E. Draper, Phys. Rev. C 1, 1069 (1970).

[4]G. L. Smith and J. E. Draper, Phys. Rev. C 1, 1548 (1970).

[5]J. E. Draper and W. Wyckoff, to be published.

[6]G. Malmsten, O. Nilsson and I. Andersson, Ark. Fys. 33, 361 (1967).

[7]R. S. Hager and E. C. Seltzer, Nucl. Data A4, 1 (1968).

[8]J. E. Draper and S. Johnsen, unpublished tables.

[9]R. M. Steffen, Purdue University Physics Report No. COO-1746-26, 1969 (unpublished).

[10]J. E. Draper and R. M. Lieder, Nucl. Phys. A141, 211 (1970).

[11]W. G. Wyckoff, Ph.D. dissertation, November, 1971 (unpublished).

[12]J. E. Draper, N. S. P. King, and W. G. Wyckoff, Bull. Am. Phys. Soc. 17, 908 (1972).

[13]J. R. Van Hise and C. Paperiello, Nucl. Phys. A188, 148 (1972); S. Göring and M. V. Hartrott, *ibid* A152, 241 (1970).

[14]D. K. McMillan and B. D. Pate, Nucl. Phys. A174, 604 (1971); K. Iizawa *et al.*, J. Phys. Soc. Jap. 30, 901 (1971).

[15]N. A. Morcos, T. E. Ward, and P. K. Kuroda, Nucl. Phys. A168, 561 (1971); T. Paradellis and S. Hontzeas, *ibid.* A142, 204 (1970).

[16]T. Hattula, S. Andre, F. Schissler, and A. Moussa, Nucl. Phys. A158, 625 (1970).

[17]E. H. Spejewski, P. K. Hopke, and F. W. Loeser, Jr., Phys. Rev. 186, 1270 (1969).

[18]A. Kerek, Nucl. Phys. A176, 466 (1971).

[19]Zh. T. Zhelev, N. G. Zaitseva, and S. S. Sabirov, Izv. Akad. Nauk SSSR, Ser. Fiz. 35, 43 (1971) [transl.: Bull. Acad. Sci. USSR Phys. Ser. 35, 40 (1971)].

[20]R. C. Ragaini, W. B. Walters, and R. A. Meyer, Phys. Rev. 187, 1721 (1969).

[21]P. R. Christensen, G. Lovhoiden, and J. Rasmussen, Nucl. Phys. A149, 302 (1970).

[22]V. P. Afanas'ev, V. S. Buttsev, I. I. Gromova, V. G. Kalinnikov, and N. A. Tikhonov, Izv. Akad. Nauk SSSR, Ser. Fiz. 35, 1603 (1971) [transl.: Bull. Acad. Sci. USSR Phys. Ser. 35, 1462 (1971)].

[23]G. L. Smith, W. Wyckoff, and J. E. Draper, unpublished tables (1970).

[24]T. Yamazaki, Nucl. Data A3, 1 (1967).

[25]M. A. J. Mariscotti, G. Scharff-Goldhaber, and B. Buck, Phys. Rev. 178, 1864 (1969).

[26]J. E. Draper, Phys. Lett. 41B, 105 (1972).

[27]G. Scharff-Goldhaber and A. S. Goldhaber, Phys. Rev. Lett. 24, 1349 (1970).